Title

A Tunable Hemispherical Platform for Non-Stretching Curved Flexible Electronics and Optoelectronics

Journal

Journal of Applied Physics, 116

Author

Ju, Y. Sungtaek

Publication Date

2014-07-01

Peer reviewed

A Tunable Hemispherical Platform for Non-Stretching Curved Flexible Electronics and Optoelectronics

Jinda Zhuang and Y. Sungtaek Ju[a)]

Mechanical and Aerospace Engineering Department, University of California, 420 Westwood Plaza, Los Angeles, CA 90095, U.S.A.

Abstract

One major challenge in incorporating flexible electronics or optoelectronics on curved surfaces is the requirement of significant stretchability. We report a tunable platform for incorporating flexible and yet *non-stretching* device layers on a hemisphere. In this configuration, an array of planar petals contractively maps onto the surface of an inflatable hemisphere through elastocapillary interactions mediated by an interface liquid. A mechanical model is developed to elucidate the dependence of the conformality of the petal structures on their elastic modulus and thickness and the liquid surface tension. The modeling results are validated against experimental results obtained using petal structures of different thicknesses, restoring elastic spring elements of different spring constants, and liquids with different surface tension coefficients. Our platform will enable facile integration of *non-stretching* electronic and optoelectronic components prepared using established planar fabrication techniques on tunable hemispherical surfaces.

a) corresponding author: Tel) +1-310-825-0985, email) just@seas.ucla.edu

1. Introduction

There recently have been growing interests in so-called flexible electronics and optoelectronics for a wide variety of applications, in particular, smart biomedical devices, biomimetic imaging devices,[1,2] wearable electronics, and robotics.[3] Some classes of the flexible device concepts, such as spherically curved focal plane detector arrays, require fabrication of electronics and optoelectronics on spherical surfaces. Such non-planar geometry is difficult to achieve in part because of the intrinsically planar nature of established micromachining techniques for semiconductor devices.

To deform a planar substrate into a spherical shape, one must stretch the center of the substrate isotropically and/or compress its perimeter tangentially. This is problematic because the resulting strains exceed the yield or fracture strength of most materials. To circumvent this issue, previous studies had to adopt a complex and challenging lift-off process sequence[4] or relied on "stretchable" conductors, such as thin interconnections that bend out of their planes, to accommodate the large strains.[1,5–7] These highly customized fabrication and integration strategies may lead to increased costs and degraded mechanical reliability/performance (e.g., fill factor) of target devices and systems.

It is therefore of great interest to develop alternative mechanical architectures for spherical electronics or optoelectronics that utilize *non-stretching* substrates and conductors while still taking full advantage of established planar fabrication processes. In this article, we report the design, micro-mechanical modeling, and experimental validation of an alternative architecture based on the contractive wrapping for possible applications in *tunable hemispherical* electronics. The architecture exploits high conformality and bendability of ultra-thin plastic, metal, or paper

substrates and can deliver tunability often reserved only for devices incorporating stretchable substrates/conductors.

2. Tunable Platform Design

A basic design of our tunable hemi-spherical device is schematically illustrated in Fig. 1. Its main component is a flexible membrane (for example, a thin polyimide layer in the present study) that is patterned into a radial array of petals and then bends to wrap a hemisphere (Fig. 1a).

In conventional origami, a flat polygon of paper is folded along creases into a 3D object, a process that may be represented mathematically as a non-crossing isometric mapping. There, however, is no isometric folding of a flat surface into an object with infinitely many points of non-zero Gaussian curvature, such as a sphere. One approach to approximate a sphere is based on contractive wrapping.[8] In the petal wrappings employed in the present study, the contours of the petals are defined as

$$b = \tan^{-1} (\sin c \tan (\pi/n)) \qquad (1)$$

Here, b is the angular width of the petal at an angular location c ($0 \leqslant c \leqslant \pi$) measured along the meridian and n is the number of the petals used to approximate a sphere (Fig. 1a). The length contraction can be achieved by forming continuous infinitesimal crinkling, by juxtaposing "semi"-flat triangles like in a geodesic dome[9], or by targeting a sphere of slightly larger diameter although at the expense of leaving finite gaps between some of the petals. The third approach is adopted here.

In the present implementation, a tunable hemisphere is formed and actuated by pneumatically inflating an elastomer membrane made of polydimethylsiloxane (PDMS). As depicted in Fig. 1c, the elastomer membrane is sandwiched between two clamping metal plates. The top plate has a center hole of radius *R* to define the hemisphere and the bottom plate has a small gas inlet for actuation. The capillary force exerted by a liquid confined in the gap between the elastomer membrane and each of the petals is used to maintain conformal contact while allowing the petals to glide freely on the elastomer membrane and the top metal plate as the elastomer membrane is inflated or deflated. The petals can *reversibly* return to their planar states when the elastomer membrane is deflated through the action of the peripheral elastic spring elements shown in Fig. 1. The elastic spring elements are made by bonding elastomeric joints on pre-folded segments of the polyimide film.

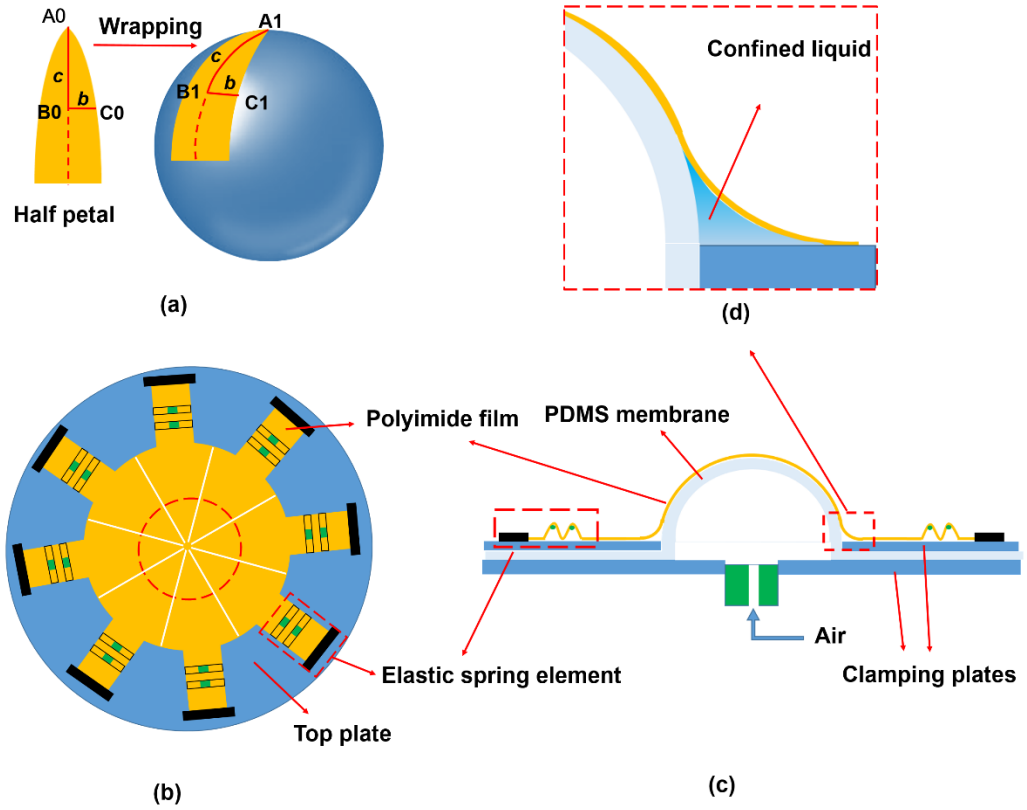

Figure 1 (color online): Conceptual design of the tunable hemispherical platform: (a) A single petal in its flat state and in its bent state to contractively map the surface of a hemisphere. (b) Top view of the tunable hemisphere platform with an array of the petals. (c) Side view of the hemisphere (d) Zoomed view near the edge of the hemisphere. The petal structures shown in (b, c) include extended strips that accommodate the elastic spring elements.

Figure 2a shows an optical image of the fabricated tunable hemispherical platform. An array of eight polyimide petals is conformally mapped on the surface of the elastomer membrane. As discussed before, small but finite gaps between the petals were intentionally incorporated into the design to eliminate crinkling or bulging associated with contractive mapping.

For further illustration, we also present in Fig. 2b a separate side view of a single isolated petal on the surface of a fully inflated elastomer membrane. The upper and middle portions of the petal are in good conformal contact with the elastomer membrane whereas the lower portion is lifted away from the membrane. The lower portion still maintains contact with the elastomer membrane and the top metal plate via a liquid bridge through its capillary interactions.

In actual integration of optoelectronic or electronic devices, one may first fabricate the devices using established planar fabrication techniques and then transfer bond them on petals made of thin polyimide films or comparable flexible "substrates." These petals are then mounted on the tunable hemisphere platform using a non-volatile liquid with negligible vapor pressure, such as ionic liquids.

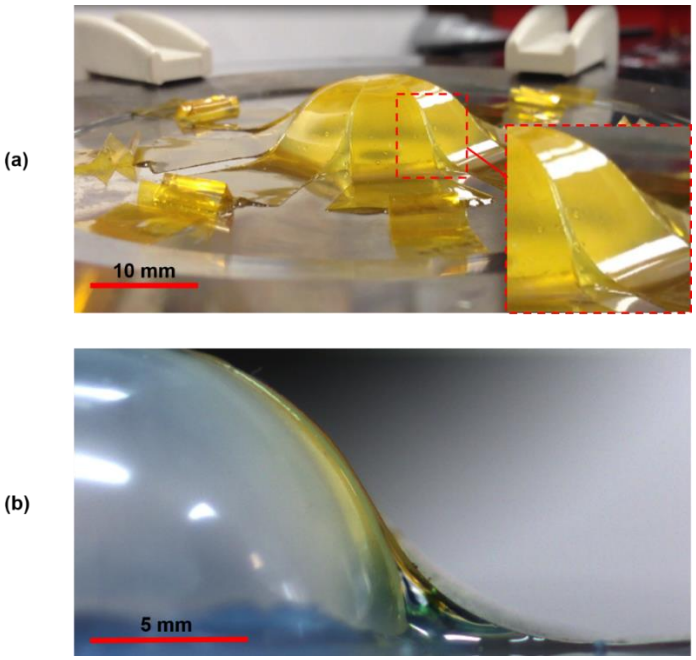

Figure 2 (color online): (a) Optical image of the tunable hemispherical platform with an array of 8 petals in contact with an inflated elastomer membrane. The inset shows a zoomed view of the two adjacent petals. (b) The contour of a single isolated petal on the surfaces of a fully inflated elastomer hemisphere and the top metal plate.

3. Mechanical Model

A mechanical model is developed to predict the geometric contour of a single polyimide petal bent under elastocapillary interactions on the inflated elastomer membrane surface. As illustrated in Fig. 3a, the bent petal structure is approximated as two arc segments AB and BC with a radius of curvature R and r, respectively. The coverage angle θ of the petal segment AB is used as a quantitative measure of the conformality of the petals. The coverage angle and the two radii of curvature are interrelated: $r(1-\cos(\theta)) = R\cos(\theta)$. We determine the coverage angle θ from the minimization of the total energy, which is the sum of the elastic energy E_e and the interfacial energy E_s.

The elastic energy E_e, which is a sum of the strain energy of the bent petal and the elastic energy of the elastic spring element, is written as

$$E_e = \frac{2B_P}{R^2} S_{AB} + \frac{B_P}{r^2} S_{BC} + \frac{k}{2} dl^2 \quad (2)$$

Here, the arc segment AB is modeled as a thin shell with the principal curvature equal to $1/R$ and the arc segment BC is modeled with a curvature of $1/r$. The bending stiffness B_P for a film of thickness h, elastic modulus E_P, and Poisson ratio ν is $B_p = E_p h^3/12(1-\nu^2)$. The net horizontal elongation of the elastic spring element dl is given as

$$dl = l_{AB} + l_{BC} - l_{OC} = (R+r)(\theta - \sin(\theta)) \quad (3)$$

The interfacial energy of the liquid in the gap E_s is approximated by ignoring variations in the curvature along the long edges of the petal (Fig. 3b) as

$$E_s = \alpha\gamma_{\mathrm{lg}}\left[2r^2(\tan(\frac{\theta}{2}) - \frac{\theta}{2}) + S_{AB} + S_{BC}\right] \quad (4)$$

where γ_{lg} is the surface tension of the liquid in the unit of N/m. The associated interface areas S_{AB} and S_{BC} are obtained from

$$\begin{aligned} S_{AB} &= R^2\int_0^{\theta} b(c)dc \\ S_{BC} &= R^2\int_{\theta}^{\theta'} b(c)dc \end{aligned} \quad (5)$$

where $\theta' = l_{\mathrm{AC}}/R$ and b is the angular width of the petal that varies as a function of the meridian coordinate c as shown in Eq. (1) and Fig. 1. The liquid wetting factor α is defined as the ratio of the wetted surface area S_{CD} of the petal segment CD to the sum of the petal surface area S_{BC} and the air-liquid interface area at the gap S_{CDE}: $\alpha = S_{\mathrm{CD}}/(S_{\mathrm{BC}}+S_{\mathrm{CDE}})$.

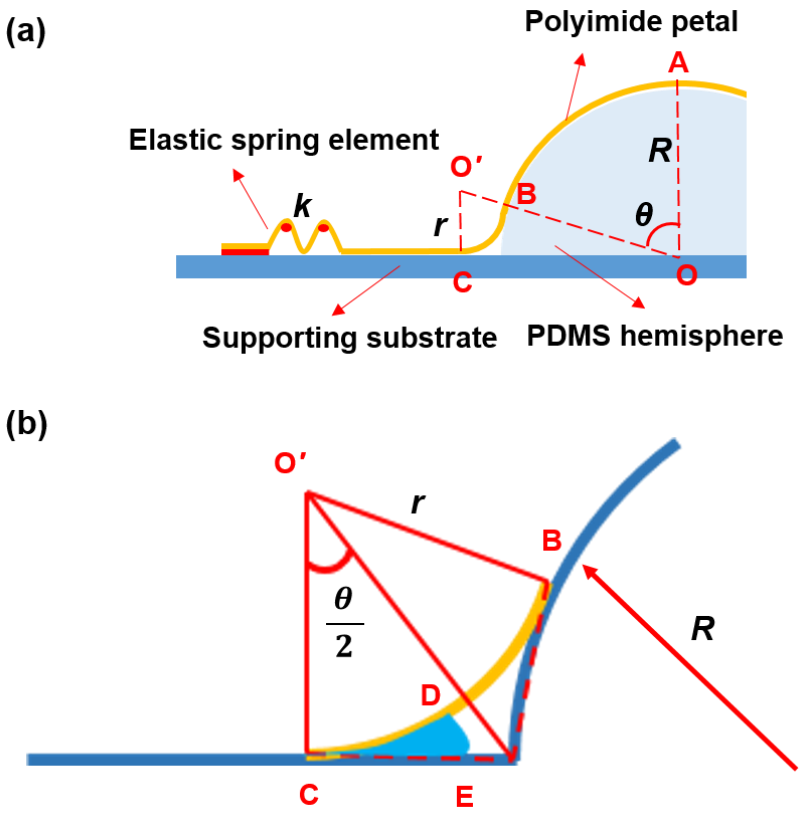

Figure 3 (color online): A geometric model of a petal structure and an elastic spring element designed to reversibly wrap the hemisphere through contractive mapping.

4. Experimental

To experimentally validate our model, we prepared thin polyimide films of varying thicknesses (3.6 ~ 12.7 μm) by spin coating a precursor solution (PI-2545, HD MicroSystems^{TM}) on a glass substrate at different speeds, curing them at 250 °C for 30 minutes, and then baking them for another 30 minutes at 350 °C. The polyimide film has an elastic modulus of 2.5 GPa and a Poisson's ratio of 0.34.

Each of the cured polyimide films was peeled off from the glass substrate and cut into the petal structure with extended strips where elastic spring elements were to be formed. One such

patterned polyimide film was mounted on the actuation platform incorporating an inflatable elastomer membrane. A liquid was next applied to fill the gap between the polyimide petals and the elastomer membrane. For a given petal structure connected to an elastic spring element with a given spring constant, we performed experiments using three different liquids: water, glycerin and silicone oil with a surface tension coefficient γ_{lg} of 73 mN/m, 64 mN/m, and 20 mN/m, respectively. In each set of experiments, a set volume of liquid was first applied using a pipette. Additional amounts of the liquid were then added in a small increment to investigate the effect of the total liquid volume. A digital camera was used to capture the profiles of the polyimide petal under given experimental conditions, which were then analyzed using ImageJ. The spring constants of the elastic spring elements were measured independently by mounting each element between a mechanical stage and an analytic balance.

5. Results and Discussion

The elastocapillary length $L_{ec} = (B_P/\alpha\gamma_{lg})^{1/2}$ is used to describe the deformation of the polyimide petals under capillary interactions.[10] It can be roughly interpreted as a measure of the length of the polyimide petal segment that can stay flat (due to elasticity) while counteracting the capillary forces. To make our model for hemispherical platforms more generally applicable, we non-dimensionalize the hemisphere radius R and liquid volume V using the elastocapillary length L_{ec}: $\bar{R} = R/L_{ec}$ and $\bar{V} = V/L_{ec}^3$.

The contour of the polyimide petal structure is governed not only by the elastocapillary interactions but also by the elasticity of the spring element. For a given spring constant k of the spring element, the smaller the elastocapillary length L_{ec} is, the larger the coverage angle θ is.

Figure 4 shows the modeled and experimentally measured coverage angles as a function of the normalized radius of the hemisphere. Larger normalized hemisphere radii (or smaller L_{ec}) result in larger values of θ, signifying better conformality. The spring element counteracts the capillary forces exerted on the petal, effectively increasing the elastocapillary length. The coverage angle, therefore, is reduced as the spring constant of the elastic spring element increases (Figs. 4 and 5). Our approximate analytic model captures the two trends observed experimentally reasonably well.

The capillary effect itself is mainly a function of the surface tension coefficient γ_g. The higher the surface tension coefficient is, the larger the elastocapillary length is. As a result, the petal has larger coverage angles for liquids with higher surface tension coefficients as illustrated in Fig. 5.

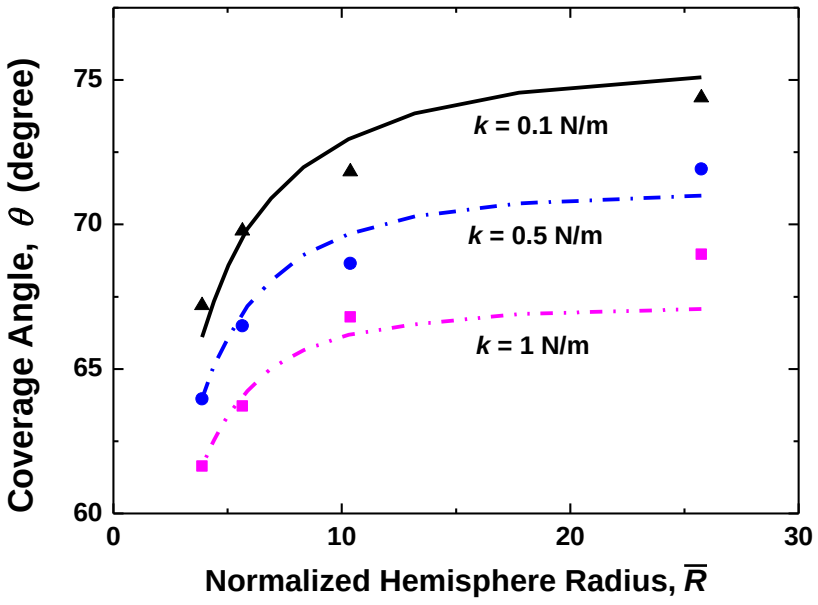

Figure 4 (color online): Modeling (lines) and experimental (symbols) results of the coverage angle θ for different values of the spring constant k. The results are plotted as a function of the normalized hemisphere radius $\bar{R}$.

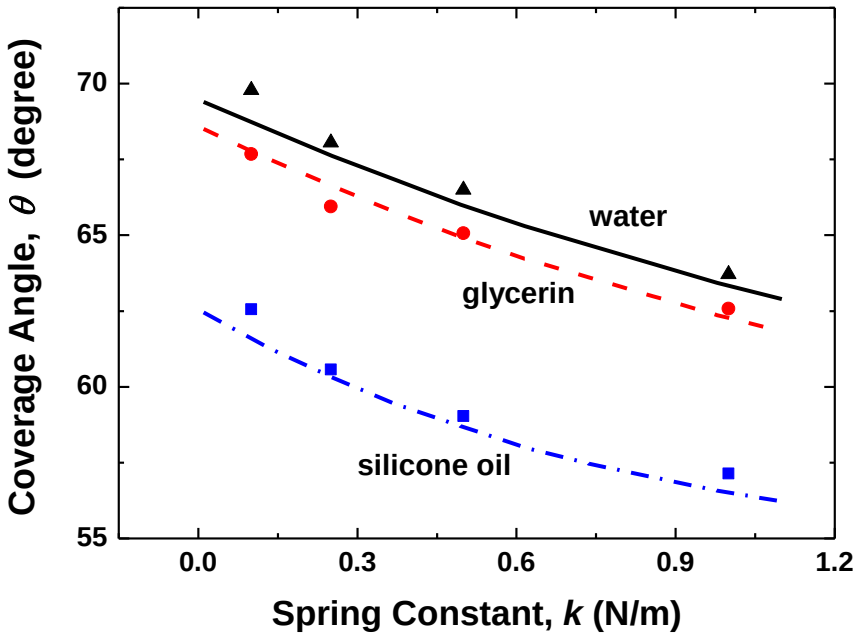

Figure 5 (color online): Modeling (lines) and experimental (symbols) results of the coverage angle θ for different liquids. The results are plotted as a function of the spring constant k of the elastic spring elements. The normalized hemisphere radii $\bar{R}$ are 5.5, 5.2 and 2.9 for water, glycerin and silicone oil, respectively.

The liquid confined in the gap between the petal and the elastomer membrane forms liquid bridges with different shapes and wetting areas for different volumes of the liquid. When the liquid volume is insufficient to fill the entire gap, disconnected liquid bridges are formed around the edge of the hemisphere. As the liquid volume is increased, a larger area of the petal is wet. The increased wetting factor α leads to a smaller elastocapillary length, which in turn results in a larger coverage angle. Referring back to Fig. 3, we note that although both the wetted petal surface area S_{CD} and the liquid-gas interface area S_{CDE} increase with the liquid volume V, the former is much larger and therefore has a larger effect on the liquid wetting factor.

At sufficiently large liquid volumes, the entire petal structures are wetted by the liquid and thus the wetted petal surface area S_{CD} remains constant. Any accumulation of the excess liquid in the gap causes the coverage angle to decrease with further increase in the liquid volume. The model prediction once again agrees well with the experimental data as shown in Fig. 6.

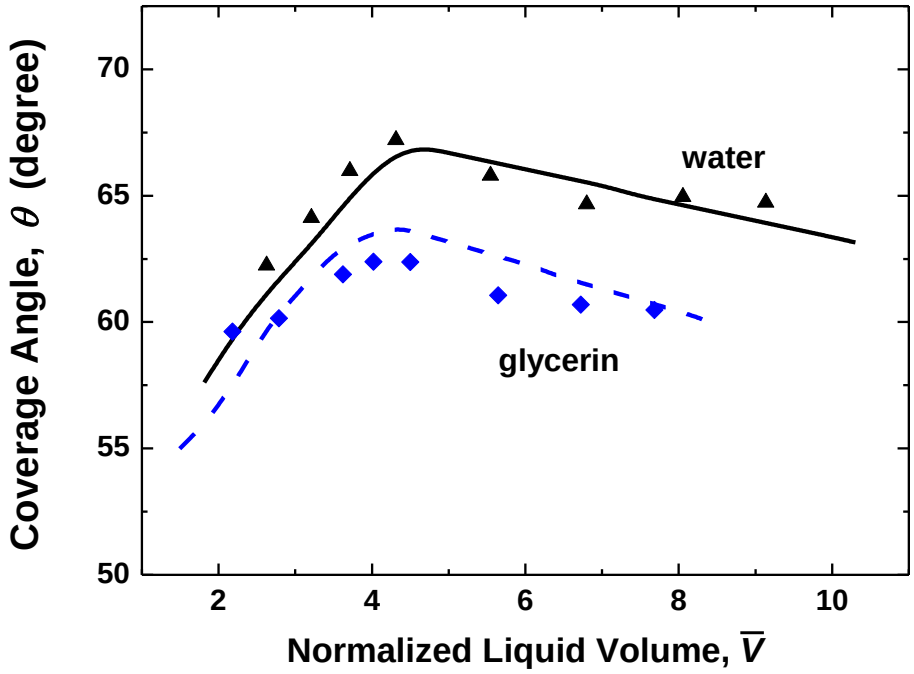

Figure 6 (color online): Modeling and experimental results of the coverage angle θ as a function of the normalized liquid volume $\bar{V}$ for two different liquids. The normalized hemisphere radii $\bar{R}$ are 5.5 and 5.2 for water and glycerin, respectively.

We use the coverage angle θ as a quantitative measure of the conformality of the petal. This coverage angle is governed by the normalized radius $\bar{R}$ and the spring constant k of the elastic spring element. For a given bending stiffness of the petal, one reaches a maximum coverage

angle θ_m (or a minimum radius of curvature r_m) when $k = 0$. This extreme condition allows us to separately illustrate the intrinsic effect of the bending stiffness on the conformality of the petal.

Figure 7 shows this theoretical maximum coverage angle θ_m as a function of the bending stiffness for two different liquids. From this plot one can determine the upper limit of the bending stiffness for a targeted coverage angle. The actual limit for elastic spring elements with finite spring constants will be lower. The limit on the bending stiffness in turn constrains the acceptable elastic modulus and/or thickness of the petal.

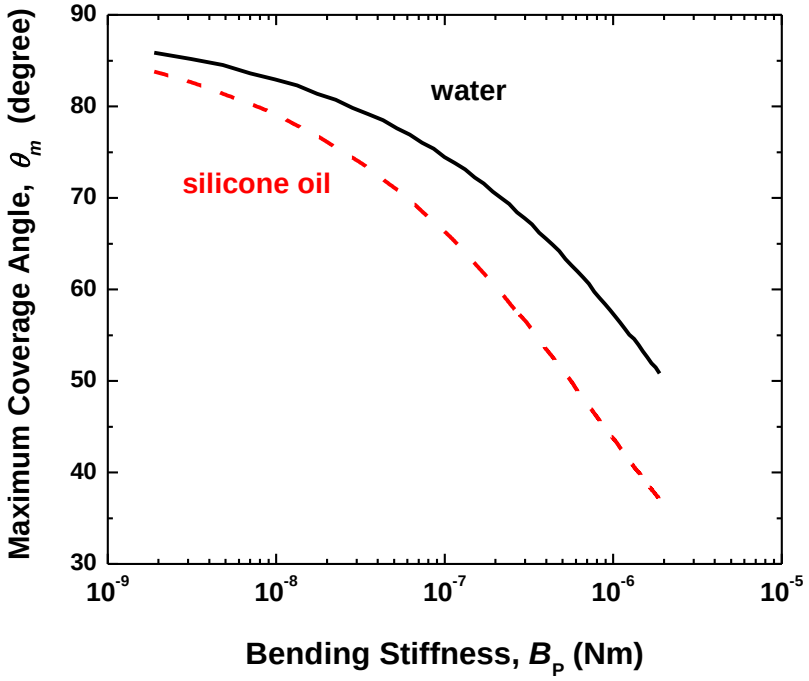

Figure 7 (color online): Theoretical predicted values of the maximum coverage angle θ as a function of bending stiffness B_P for two different liquids.

Figure 8 shows the normalized radius as a function of bending stiffness for water and silicone oil. The bending stiffness once again is given as $B_p = E_p h^3/12(1-\nu^2)$. The elastic moduli of common flexible polymeric or rubbery materials are of the order of 100 MPa. With minimum

practical layer thicknesses of the order of 1 μm, one has a practical lower bound in the bending stiffness of the order of 10^{-10} N m. As a practical upper bound, bending stiffness values of the order of 10^{-3} N m are obtained for very "stiff" films of thickness 50 μm and elastic modulus 100 GPa.

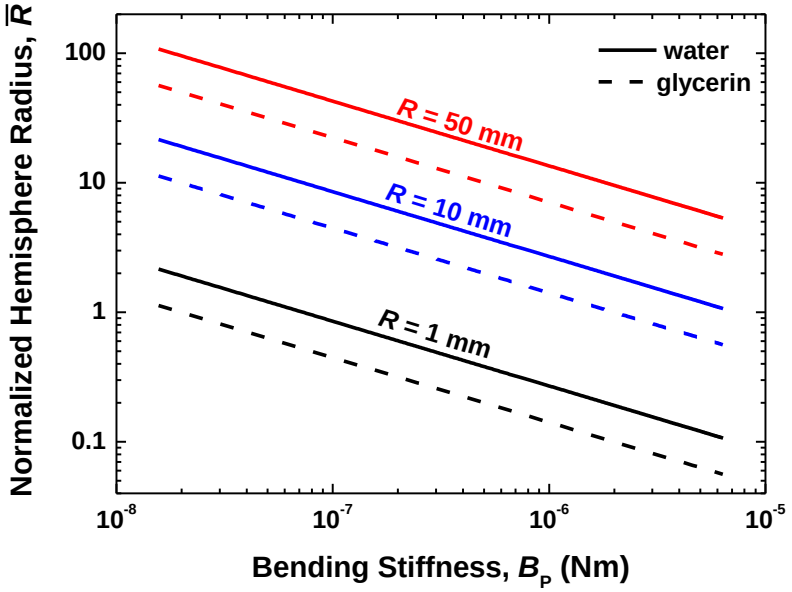

Figure 8 (color online): The normalized radius $\bar{R}$ as a function of bending stiffness B_p for different values of the hemisphere radius R.

When designing of a specific system, one needs to choose combinations of the normalized hemisphere radius $\bar{R}$ and the spring constant k consistent with a targeted value of the coverage angle. Figure 7 provides the maximum possible coverage angle, which one may achieve in the limit $k = 0$. In practice, the elastic spring elements with a finite spring constant ($k \neq 0$) are necessary to provide restoring forces and achieve reversible operations. Figure 9 shows predicted contour lines of the coverage angle as a function of the normalized hemisphere radius

$\bar{R}$ and the spring constant k. For each contour line (that is, for a given targeted coverage angle), the normalized hemisphere radius increases with the spring constant and diverges when the spring constant reaches a certain critical value.

When the spring constant is relatively small (as an example, Region I for $\theta = 70°$ in Fig. 9), the required normalized hemisphere radii are small and hence the petal bending stiffness B_p can be large. Recall that $\bar{R} \sim R / B_p^{0.5}$. The "soft" elastic springs ($k < 0.1$ N/m), however, may not provide sufficient restoring forces for reliable reversible operations. In the opposite limit of very "stiff" elastic spring elements (Region III in Fig. 9), the required normalized hemisphere radii are large and hence the petal bending stiffness B_p must be small. In this region, petals can only be made of very flexible materials with small elastic moduli and/or have very small thicknesses.

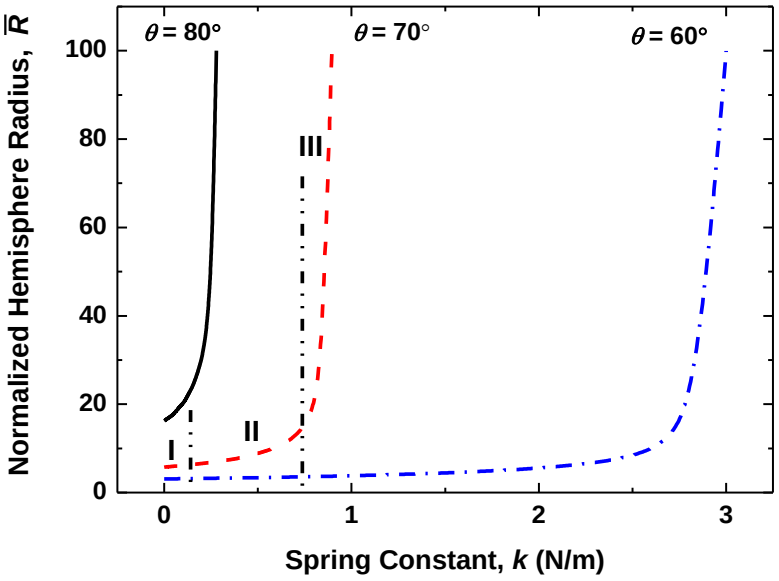

Figure 9 (color online): Theoretical predictions of the normalized radius $\bar{R}$ as a function of spring constant k for different values of the coverage angle θ.

In summary, a mechanical design of a tunable hemispherical platform for non-stretching substrates is reported for possible flexible electronic and optoelectronic applications. The tunable transformation of a planar substrate incorporating electronic or optoelectronic components into a hemisphere is achieved via contractive wrapping of petal-shaped structures on a pneumatically actuated elastomeric membrane. The conformality of the film wrapping on the hemispherical elastomer surface under various circumstances is predicted using an analytical model accounting for elasto-capillary interactions. The predicted values of the coverage angle and its dependence on the design parameters (the bending stiffness of the petal, the surface tension of the interface liquid, and the spring constant of the elastic spring elements) all show good agreement with our experimental results. This study demonstrates the early feasibility of such non-stretching mechanical architectures for use in tunable hemispherical opto-electronic and other related devices and provides possible design parameter spaces.

References

[1] Y.M. Song, Y. Xie, V. Malyarchuk, J. Xiao, I. Jung, K.-J. Choi, Z. Liu, H. Park, C. Lu, R.-H. Kim, R. Li, K.B. Crozier, Y. Huang, and J.A. Rogers, Nature **497**, 95 (2013).

[2] D. Floreano, R. Pericet-Camara, S. Viollet, F. Ruffier, A. Brückner, R. Leitel, W. Buss, M. Menouni, F. Expert, R. Juston, M.K. Dobrzynski, G. L'Eplattenier, F. Recktenwald, H.A. Mallot, and N. Franceschini, Proc. Natl. Acad. Sci. **110**, 9267 (2013).

[3] M. Kaltenbrunner, T. Sekitani, J. Reeder, T. Yokota, K. Kuribara, T. Tokuhara, M. Drack, R. Schwödiauer, I. Graz, S. Bauer-Gogonea, S. Bauer, and T. Someya, Nature **499**, 458 (2013).

[4] P.I. Hsu, R. Bhattacharya, H. Gleskova, M. Huang, Z. Xi, Z. Suo, S. Wagner, and J.C. Sturm, Appl. Phys. Lett. **81**, 1723 (2002).

[5] P.J. Hung, K. Jeong, G.L. Liu, and L.P. Lee, Appl. Phys. Lett. **85**, 6051 (2004).

[6] R. Dinyari, S.-B. Rim, K. Huang, P.B. Catrysse, and P. Peumans, Appl. Phys. Lett. **92**, 091114 (2008).

[7] G. Shin, I. Jung, V. Malyarchuk, J. Song, S. Wang, H.C. Ko, Y. Huang, J.S. Ha, and J.A. Rogers, Small **6**, 851 (2010).

[8] E.D. Demaine, M.L. Demaine, J. Iacono, and S. Langerman, Comput. Geom. **42**, 748 (2009).

[9] R.A. Street, W.S. Wong, and R. Lujan, J. Appl. Phys. **105**, 104504 (2009).

[10] B. Roman and J. Bico, J. Phys. Condens. Matter **22**, 493101 (2010).

Figure Captions

Figure 1 (color online): Conceptual design of the tunable hemispherical platform: (a) A single petal in its flat state and in its bent state to contractively map the surface of a hemisphere. (b) Top view of the tunable hemisphere platform with an array of the petals. (c) Side view of the hemisphere (d) Zoomed view near the edge of the hemisphere. The petal structures shown in (b, c) include extended strips that accommodate the elastic spring elements.

Figure 2 (color online): (a) Optical image of the tunable hemispherical platform with an array of 8 petals in contact with an inflated elastomer membrane. The inset shows a zoomed view of the two adjacent petals. (b) The contour of a single isolated petal on the surfaces of a fully inflated elastomer hemisphere and the top metal plate.

Figure 3 (color online): A geometric model of a petal structure and an elastic spring element designed to reversibly wrap the hemisphere through contractive mapping.

Figure 4 (color online): Modeling (lines) and experimental (symbols) results of the coverage angle θ for different values of the spring constant k. The results are plotted as a function of the normalized hemisphere radius $\bar{R}$.

Figure 5 (color online): Modeling (lines) and experimental (symbols) results of the coverage angle θ for different liquids. The results are plotted as a function of the spring constant k of the

elastic spring elements. The normalized hemisphere radii $\bar{R}$ are 5.5, 5.2 and 2.9 for water, glycerin and silicone oil, respectively.

Figure 6 (color online): Modeling and experimental results of the coverage angle θ as a function of the normalized liquid volume $\bar{V}$ for two different liquids. The normalized hemisphere radii $\bar{R}$ are 5.5 and 5.2 for water and glycerin, respectively.

Figure 7 (color online): Theoretical predicted values of the maximum coverage angle θ as a function of bending stiffness B_{P} for two different liquids.

Figure 8 (color online): The normalized radius $\bar{R}$ as a function of bending stiffness B_{p} for different values of the hemisphere radius R.

Figure 9 (color online): Theoretical predictions of the normalized radius $\bar{R}$ as a function of spring constant k for different values of the coverage angle θ.